OATAO is an open access repository that collects the work of Toulouse researchers and makes it freely available over the web where possible

This is an author's version published in: http://oatao.univ-toulouse.fr/28683

Official URL:

https://doi.org/10.1109/TCPMT.2021.3074652

To cite this version:

Khazaka, Rabih and Martin, Elodie and Alexis, Joël and Martineau, Donatien and Azzopardi, Stephane *Evaluation of direct printed heat sinks on metallized ceramic substrate for high-performance power modules.* (2021) IEEE Transactions on Components, Packaging and Manufacturing Technology, 11 (6). 955-962. ISSN 2156-3950

Any correspondence concerning this service should be sent to the repository administrator: tech-oatao@listes-diff.inp-toulouse.fr

Evaluation of Direct Printed Heat Sinks on Metallized Ceramic Substrate for High-Performance Power Modules

Rabih Khazaka, Elodie Martin, Joel Alexis, Donatien Martineau, and Stephane Azzopardi

***Abstract*— In this article, we propose a new packaging technology enabling the development of a high-performance power module for harsh environments. This approach is based on the use of the selective laser melting (SLM) technique in order to directly print metal heat sinks on the backside of the metallized substrate. In order to explore the viability of this method, the assembled parts were evaluated thoroughly after the manufacturing process. Moreover, their robustness was assessed during aging under harsh conditions. Results show that the ultimate tensile strength and yield strength of the printed alloy are higher than the casted $AlSi_7Mg_{0.6}$ counterpart. The interfaces between the printed alloy and the substrate Al metal layer do not show any weaknesses, and shear stress values are higher than 100 MPa. For all heat sink patterns, the substrate warpage is reduced during thermal cycling due to the Al alloy creeping, while the highly curved substrates show cracks in the ceramic after 400 cycles. Accordingly, direct printing of heat sink with patterns based on fins array reveals a promising path for high-reliability, high-performance power module packaging.**

***Index Terms*— $AlSi_7Mg_{0.6}$ alloy, direct printed heat sink, power module packaging, robustness, selective laser melting (SLM).**

I. Introduction

In the last decades, the electrification of aircraft has drawn considerable attention. The main objectives are the improvement of reliability, efficiency, and flexibility while reducing weight and greenhouse gas emissions. Recently, in electric aircraft technology, the mechanically driven engine accessories (oil pump, fuel pump, hydraulic pump, and so on) and pneumatic and hydraulic systems are gradually replaced with electrically driven versions. Electric actuators and machine control are often based on power electronics converters in which the power module is a critical component. This latter ensures electrical connections between the devices and the external electrical connectors, heat management, and the mechanical robustness of the package. The use of high-density integrated power modules is of utmost importance to achieved mass and volume gain. Thus, a higher amount of heat density requires to be dissipated, and more robust technologies need to be implemented. This trend is mainly driven by the market introduction of high-temperature wide bandgap power semiconductor devices, such as silicon carbide (SiC) or gallium nitride (GaN), with junction temperature exceeding 200 °C [1]–[3]. However, to complete this breakthrough, the entire packaging system of the component must be rethought.

Rabih Khazaka, Donatien Martineau, and Stephane Azzopardi are with the Electrical and Electronic Systems Research Group, Safran Tech, 78114 Magny-Les-Hameaux, France (e-mail: rabih.khazaka@safrangroup.com).

Elodie Martin is with the Aeronautics, Space and Defense Division, Altran, 75017 Paris, France

Joel Alexis is with the Production Engineering Laboratory (LGP), INP-ENIT, 65016 Tarbes, France

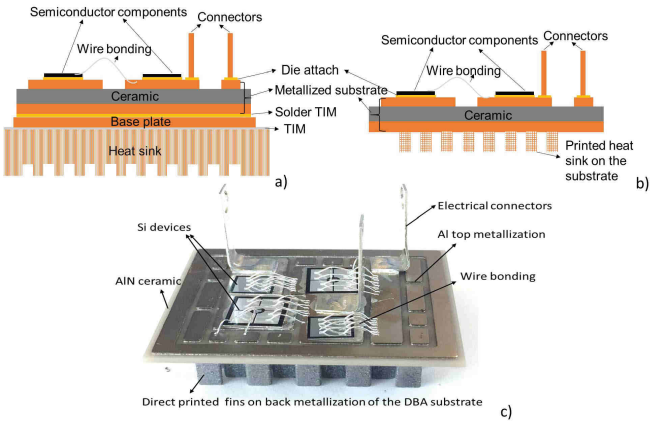

Fig. 1. Schematic view of (a) conventional power module packaging cross section and (b) proposed structure. Single-phase leg inverter with two IGBTs and two diodes assembled on the DBA substrate. (c) Fins array have directly been printed on the backside metallization before attaching the devices.

In conventional module assembly presented in Fig. 1(a), the power devices of the module are attached to the substrate mainly by the use of solder. Recently developed die attach technologies, such as transient liquid-phase bonding and metal sintering, have emerged during the last decade and can allow the operation in harsh environments [4]–[6]. The substrate provides the electrical insulation and ensures the circuitry in the module through the upper metallic layout. Ceramic-based substrates with various manufacturing technologies, such as direct bonded copper (DBC), direct bonded aluminum (DBA), and active metal brazing (AMB), are commonly used, and the two latter technologies are preferred for large amplitude thermal cycles where temperature swings ΔT are higher than 200 °C [4], [7], [8]. The substrate of the conventional power

module is thermally coupled to the base plate using solder as TIM and then to the heat sinks using other TIM. In some cases, pin-fins are added directly to the base plate, and the heat sink is eliminated [9]. The solders used as TIM between the substrate and the base plate suffer from its limited reliability under large thermal cycles ($\Delta T > 200$ °C) due to the coefficient of thermal expansion (CTE) mismatch between the substrate base plate and the large bonded surface [10], [11].

The thermal coupling with the heat sink is achieved with organic materials, such as thermal greases, elastomers, or phase-changing films. The Achilles heel of such assembly is TIMs that suffer from their low thermal conductivity (<8 W·m^{-1}·K^{-1}) and limited stability at high temperatures (<150 °C) [12]. Graphite and graphene sheets are used as TIM, but low thermal conductivity in at least one direction has been always observed (anisotropic material). Therefore, flat and smooth surfaces and high pressures are required to achieve good thermal contact [13]. Finally, some technologies eliminate the thermal interface material by using direct jet impingement cooling [14], [15] or spray cooling [16], [17] on the substrate or the device. These technologies allow the TIM elimination and high heat flux dissipation. However, limited exchange surface, complex cooling systems, and the risk of plugging the nozzle head by impurities represent the main drawbacks of such technologies compared the conventional air- or liquid-cooling ones.

Recently, additive manufacturing has shown to be a growing area of research to achieve optimized high-performance heat sink designs that cannot be achieved using traditional manufacturing techniques [18]–[20]. In order to leverage additive manufacturing technologies and overcome the aforementioned limitations related to the use of TIM or the use of direct cooling technologies, a new approach is proposed and evaluated in this article. It consists of directly printing heat sinks using the selective laser melting (SLM) technique on the backside of the metallized substrate, as schematically presented in Fig. 1(b). Various conventional and less-conventional heat sink patterns have been printed. By using thermofluidic simulations, it has been shown that this approach allows the reduction of the junction to ambient thermal resistance by more than 20% [21]. An example of a single-phase leg inverter assembly on the DBA substrate with rectangular fins printed on the substrate backside metallization is illustrated in Fig. 1(c).

However, thermal performance improvement is not a unique topic and the structure where the heat sink is mechanically coupled to the substrate should be investigated. The intrinsic properties of the printed alloy should be assessed in order to ensure that the materials have acceptable thermal conductivity and can withstand mechanical solicitation (vibration, shocks, and so on). The interface quality between the printed alloy and the substrate metal layer that guarantees the mechanical and thermal coupling between the substrate and the heat sink should also be assessed, as well as the residual stresses induced in the structure at the end of the additive manufacturing process. Therefore, this article will be focused on the evaluation of the mechanical, thermal, and microstructural properties of the printed material. Special attention is dedicated to the interface properties between the printed alloy and the substrate aluminum metallization. The assembly warpage was also considered as the main concern, and the substrate camber was measured for various heat sink designs in order to establish a relationship between the printed pattern and the induced residual stress in the assembly. Finally, the robustness of the package during long-term storage at 200 °C for 1000 h and during thermal cycling between −55 °C and 200 °C was investigated.

II. Experiments

A. Samples Manufacturing

In this work, commercially available DBA metallized substrates from Denka were used. The substrates were selected for their high thermomechanical reliability, good thermal conductivity, and the compatibility of the Al metallization with the printed Al-based alloy [4], [22]. The dimensions of the AlN ceramic and Al metal layers were $48 \times 42 \times 1$ and $46 \times 40 \times 0.4$ mm^3, respectively, and the Al layers were bonded on both sides of the ceramic plates. The pattern is then formed by selective etching of the top substrate metal layer. The apparatus used to print the $AlSi_7Mg_{0.6}$ metal parts is the SLM Solutions SLM280HL 400 W with a $280 \times 280 \times 365$ mm^3 build envelope and a high-power laser beam profile. The particle size of the $AlSi_7Mg_{0.6}$ powder is in the range of 20–60 μm. The 3-D geometry is realized layer by layer using a 350-W laser power with a scan speed of 600 and 900 mm/s for the edge contour and the center of the built parts, respectively. The laser beam locally melts the powder, which is quickly solidified to form the slice. Powder layers are consequently deposited and melted until the achievement of the final design. An argon atmosphere is maintained in the chamber during the entire process in order to avoid the oxidation of metallic materials and prevent fire. To reduce the residual stresses in the final assembly, the built plate that receives the DBA substrates is heated at 150 °C. Fig. 2 shows samples used for this study. In the following, the X-axis refers to the laser scan direction in the plane of the substrate, and Z is the out-of-the-plane axis corresponding to the direction of consecutive selective melted powder layers. In order to determine the manufacturing direction impact on the sample mechanical strength, as well as interfaces between melted tracks and layers, the tensile stress has been applied in the parallel direction to the X- or Z- axis [see Fig. 2(a)]. The DBA substrates with printed rectangular fins have been used for microstructural and mechanical interface evaluation [see Fig. 2(c)], and substrates with or without heat sinks have been used for the warpage measurements.

B. Evaluation Tests

In order to evaluate the viability of the developed technology, tests are performed in order to assess the material intrinsic properties (thermal conductivity, mechanical properties, and microstructure) and the interface between the metallized substrate and the additive manufactured metal (microstructure and mechanical adhesion). In addition, since the metal powder is melted for short periods during the process, high residual stresses can be induced in the assembly during manufacturing

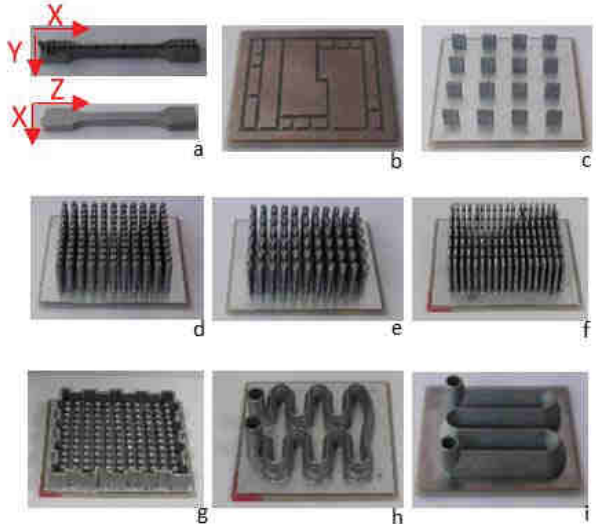

Fig. 2. (a) Free-standing samples for tensile tests (where Z corresponds to the out-of-plane axis). (b) Topside of the DBA substrate. (c) Substrate with rectangular fins used for interface evaluation (shear tests and microstructure analysis). Various heat sink patterns printed on the backside of the substrates as follows: (d) pin fins array, (e) water drop shape fins array, (f) rectangular fins array, (g) pin fins with castle-like border, (h) splined water channels, and (i) linear water channels.

and may lead to substrate cracking. This issue has been monitored using the substrate warpage measurements after the heat sink printing. Finally, the robustness of the assembly was demonstrated during high-temperature storage and thermal cycles using destructive and nondestructive tests (mechanical properties, microstructures, warpage measurements, and visual observation).

High-temperature storage was performed at 200 °C for 1000 h, while thermal cycles were applied in the range from −55 °C to 200 °C with heating and cooling ramps set at 10 °C/min and a 5-min dwell time at the maximum and minimum temperatures.

The density and specific capacity of the material have been evaluated using the mass and volume measurements and dynamic scanning calorimetry, respectively. For the thermal diffusivity, the laser flash method in the temperature range between 20 °C and 200 °C has been used. Samples used for these evaluations were printed on the substrate and then cut up with the dimensions $10 \times 10 \times 1$ mm^3. The microstructure and interface properties have been characterized using scanning electron microscopy (SEM) after sample preparation and the Keller etching. Tensile tests have been carried out to characterize the mechanical behavior of the printed $AlSi_7Mg_{0.6}$ samples in the temperature range between −50 °C and 200 °C. Shear tests are performed to evaluate the interface's mechanical behavior. In all cases, the mechanical tests were carried out with a force cell maximum value of 10 kN and a displacement speed of 1 mm/min. Three tests were performed for each condition to verify the measurements' repeatability. The warpage of the substrates has been measured on the width and the length of the substrates by using an optical profilometer in white light. For each dimension, three independent measurements (with two measurements on the borders and one on the substrate center) have been performed. The warpage values correspond to the average difference between the lowest and the highest points measured on the three deformation lines.

III. Experimental Results

A. Initial Properties of the Assembly

1) Printed Material Properties: The printed alloy density, its specific capacity, and its thermal diffusivity were 2630 kg·m^{-3}, 866 J·kg^{-1}·K^{-1}, and 0.5 cm^2·s^{-1}, respectively. The thermal conductivity λ was then calculated by multiplying the diffusivity, the density, and the specific capacity. Measurements were achieved in the temperature range between 20 °C and 200 °C. In the tested range, the thermal conductivity seems to be temperature independent with the value of 112 W·m^{-1}·K^{-1}± 3%. For comparison purposes, the density, the thermal conductivity, and the specific capacity of casted $AlSi_7Mg_{0.6}$ are 2700 kg·m^{-3}, 145 W·m^{-1}·K^{-1}, and 961 J·kg^{-1}·K^{-1}, respectively.

The microstructure of the selective laser melted alloy is presented in Fig. 3 in the plane direction (XY) and the layers' building direction (YZ). A significant ratio of porosities with a diameter of about 100 μm for the largest ones is observed. The $AlSi_7Mg_{0.6}$ fabricated using SLM presents a heterogeneous microstructure. In fact, in the XY plane, the finest structure of the cellular dendrites is observed at the center of the melting bath, and a larger dendrites size is achieved between two adjacent melting baths and at the border of the printed parts in Fig. 3(c) and (d). This can be explained by the fact that the temperature of the center of the melted bath is higher than the borders, and hence, the thermal gradient is higher. Accordingly, the temperature decrease rate during the solidification is higher leading to finer microstructure [23]. In the YZ plane, the shape of half of the circles is illustrated in Fig. 3(e), and it allows distinguishing four laser tracks in the Y-direction. This shape is frequently observed when using a unidirectional scanning strategy along the X-axis that creates parallel scans in the Y-direction [24].

Mechanical tensile tests on $AlSi_7Mg_{0.6}$ free-standing samples were achieved with a force applied in the scan direction (X-direction) and in the direction of the built layers (Z-direction). The yield strength (YS), the ultimate tensile strength (UTS), and the elongation at break are given for the temperature range of interest from −50 °C to 200 °C in Fig. 4. The measured UTS and YS are both more than 30% higher than the traditionally AlSiMg cast alloy due to three main factors [25], [26]: the ultrafine-grained microstructure favors the grain boundary strengthening, the constituent elements that induce solid solution strengthening, and the strengthening given by the interactions of dislocations. A decrease in the YS and the UTS associated with an increase in elongation at fracture is observed by increasing temperature. The dispersion in the results for the UTS and YS is less than 5%, while the elongation at break shows a variation that can reach 50% between the samples tested under the same conditions.

Both UTS and YS seem to be independent of the printing direction. The obtained results of YS and UTS are

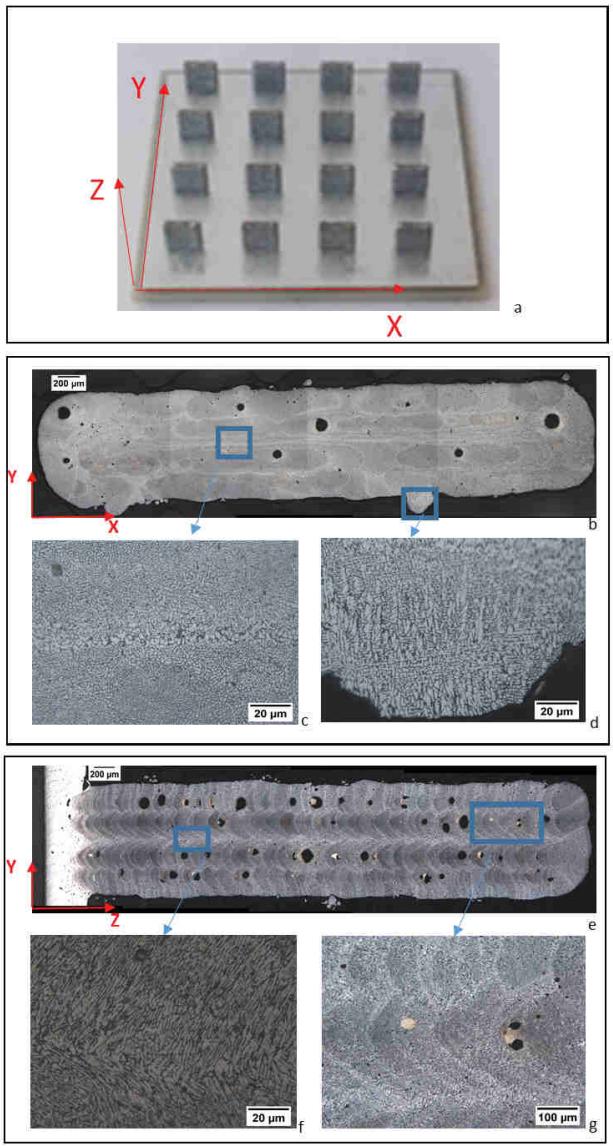

Fig. 3. 3-D image of the sample used for (a) microstructure analysis and $AlSi_7Mg_{0.6}$ microstructure after selective laser melting in (b)–(d) *XY* plane and (e)–(g) *YZ* plane.

in agreement with the ones reported in the literature for AlSiMg-based alloys, while the elongation at break seems to be lower in our samples [26], [27]. This can be attributed to the high pores' ratio that can reduce the elongation limit. In fact, pores can be considered as a weak point for fracture initiation. Their position and size can strongly impact the elongation at break, which can explain the high dispersion of the results between the samples manufactured and tested under the same conditions. Otherwise, in all the tested conditions, the fracture surfaces reflect a ductile behavior of $AlSi_7Mg_{0.6}$ alloy with the presence of dimples and a necking that increases with temperature, as illustrated in Fig. 4(c), after tensile tests at 25 °C and 200 °C.

2) Interfaces Properties: For the interface analysis, SEM images in secondary and backscattered electrons, and

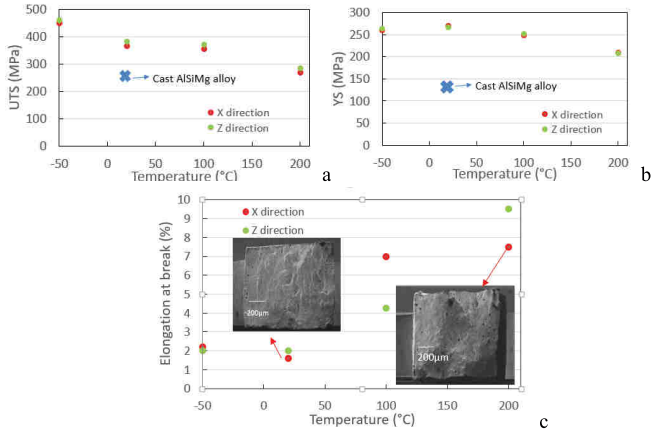

Fig. 4. (a) UTS, (b) YS, and (c) elongation at break as a function of temperature (*X* and *Z* tensile force direction) and fracture surfaces of tensile test specimens at 20 °C and 200 °C.

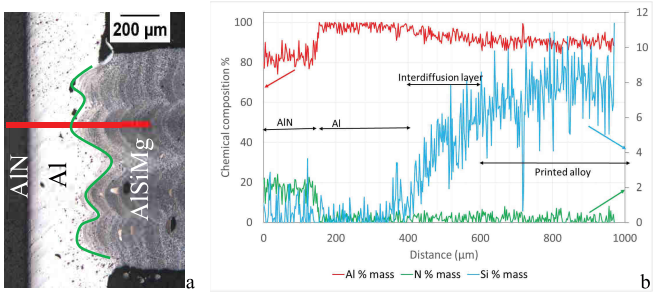

Fig. 5. (a) Interface images using backscattered electrons and (b) EDX detected element distribution on the red line on the interface image (from left to right).

energy-dispersive *X*-ray (EDX) spectroscopy, were achieved. The results are shown in Fig. 5. At the level of the diffusion layer, we can see that it is not regular over the entire interface but rather in the form of waves [green curve in Fig. 5(a)]. The maximum depth of the interdiffusion zone is about 200 μm, as detected by the silicon diffusion depth, and corresponds to the center of the melted bath where the highest temperature is reached.

Shear tests were used to evaluate the mechanical properties of the interfaces, and a shear strength value of 109 MPa was obtained. The surfaces were then analyzed by SEM and EDX and also by using profilometry analysis in order to identify the type and the location of the fracture (see Fig. 6). SEM and EDX analyses show a ductile fracture with a large amount of Al at the surface that suggests two potential failure types: a cohesive fracture in the Al or an adhesive fracture at the Al/diffusion zone interface. This result was obtained for 97% of the tested samples. The relief indicates a depth of about 250 μm. Combined with the aforementioned diffusion profile where the maximum diffusion depth of the Si is detected on the first 200 μm in the Al substrate metallization, it can be concluded that the fracture corresponds rather to a cohesive rupture in the Al substrate metallization.

3) Heat Sink Design Impact on Substrate Warpage: In order to evaluate the influence of the heat sink design on

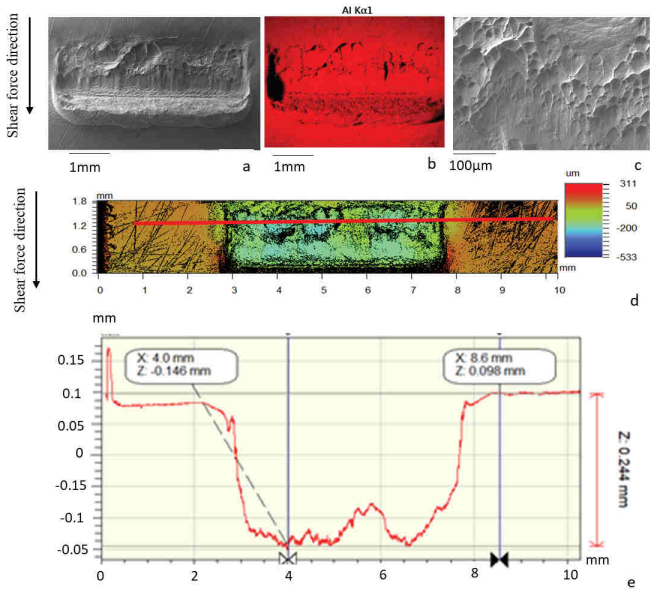

Fig. 6. (a) SEM image using secondary electrons of the fracture surface on the substrate side where the left arrow indicates the applied force direction, (b) Al detection using EDX, (c) SEM image inside the pit showing the plastic deformation of the Al, (d) optical profile of the surface showing the pit formed in the Al metal, and (e) linear profile at the red line indicated in (d) showing a maximal depth of 244 μm.

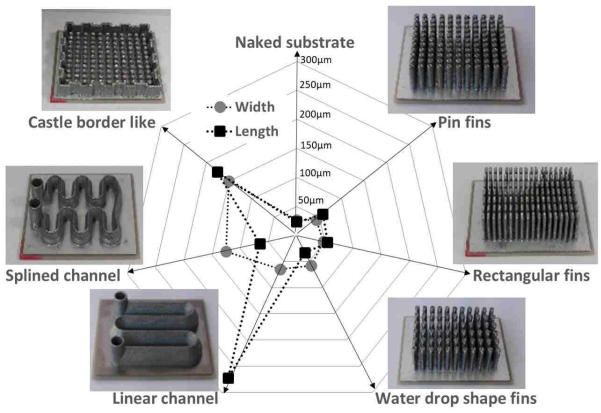

Fig. 7. Heat sink pattern impact on the substrate warpage.

the residual stresses and the deformations of the assemblies, warpage measurements on the width and on the length of the substrates were realized and are presented in Fig. 7. Results reveal that fins array heat sink patterns (rectangular fins, water drop shape fins, and pin fins) with short continuous lines on the substrate are recommended to avoid the substrate bowing and the ceramic cracking. For these patterns, the deformation of the substrate was less than 60 μm, while deformation of about 25 μm was measured for the naked substrate. When the pattern presents long linear printed vectors, substrates are highly curved. Heterogeneous deformations are observed for the geometry of spline and straight channels, and the higher deformation in both cases is observed in the direction where a continuous long vector is printed. In fact, decreasing the length of scanning vectors reduces the residual stresses and,

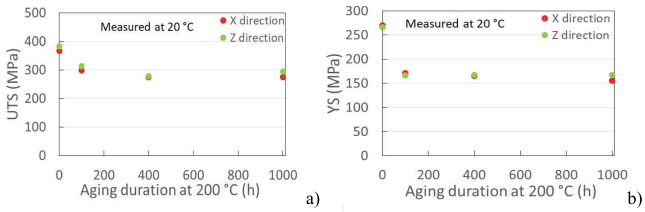

Fig. 8. (a) UTS and (b) YS measured at 20 °C as a function of storage time at 200 °C.

hence, the warpage of the substrate. This can be due to two favorable mechanisms. In fact, when short-printed vectors are used, the volume of the melted material that will solidify after the laser scan will be lower and will occur on a small surface. Hence, the mechanical stresses will be reduced and redistributed locally in the substrate plane. In addition, the use of short printing vectors with a suitable printing strategy can allow a better distribution of the heat. The time between two adjacent vectors can be sufficiently low, and the first printed vector will allow achieving a local preheating to the second one. Hence, the thermal gradient in between the second printed vector and the substrate is reduced and, consequently, the mechanical stresses.

B. Robustness Evaluation Under Harsh Aging Conditions

Compared to thermal cycles, thermal storage can induce more pronounced modification in the mechanical properties of the free-standing additive manufactured samples. However, the interface properties can be strongly related to both types of aging, while the reliability of the assembly (substrate heat sink) is mainly influenced by the thermal cycles where CTE mismatch between the various materials and the hardening of the alloy can induce severe failures. Hence, thermal storage aging was achieved on the free-standing samples and the samples dedicated for interface properties evaluation, while the latter samples and samples with heat sink patterns printed on the substrate were used for passive thermal cycles' aging.

1) Printed Material Properties During Thermal Storage Aging: At room temperature, the mechanical properties as a function of aging time achieved with a force applied in the scan direction (X-direction) and the direction on the built layers (Z-direction) are illustrated in Fig. 8. YS and UTS show a decrease of about 40% and 20%, respectively, after 100 h followed by a stabilization of the properties during the remaining aging duration. The same behavior has been reported on $AlSi_{10}Mg$ samples manufactured using the SLM technique where a slight decrease was recorded for the yield and UTSs after 2 h at 250 °C [27]. However, this variation is not considered a critical issue for our applications since the main role of the printed material is related to thermal management, and the latter will not be submitted to hard mechanical solicitations.

2) Interfaces Properties During Thermal Storage and Thermal Cycles' Aging: The metallurgical analysis was carried out during the thermal storage for 1000 h at 200 °C and during the 1000 thermal cycles from −55 °C to 200 °C. Both the

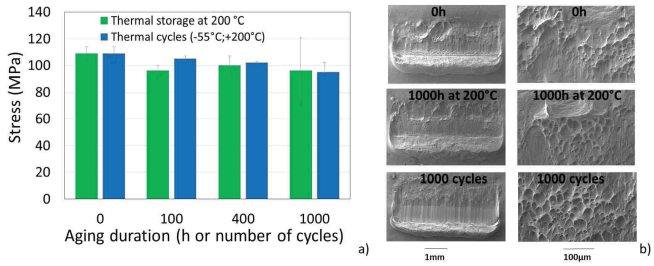

Fig. 9. (a) Shear test results at the initial state and after aging under thermal storage and thermal cycles. (b) SEM images for the surface of the fracture at the initial time and at the end of the aging tests.

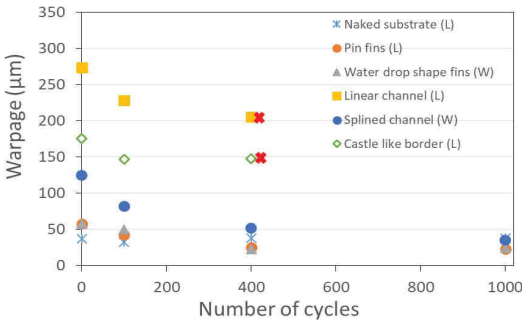

Fig. 10. Warpage evolution during aging under thermal cycles for various heat sink patterns (L: length and W: width). Red crosses indicate the detection moment of the substrate cracks.

aging conditions do not seem to have any influence on the interdiffusion phenomena, and the diffusion of the Si does not exceed half of the Al coating (200 μm). In order to validate the weak metallurgical evolutions at the interface, shear tests were performed after the thermal storage and the thermal cycles' aging, and the results are presented in Fig. 9(a). The mechanical shear strength is relatively stable, and the stress value remains above 90 MPa. The surfaces of the fracture were then studied for aged samples, and results were similar to the ones obtained before the aging, as shown in Fig. 9(b).

3) Substrate Warpage During Thermal Cycles: The goal of these tests is to evaluate the thermomechanical reliability of the assembly (substrate/heat sink). The results showing the warpage variation during the thermal cycles are presented in Fig. 10 for the highest curved dimension at the initial state (width or length depending on heat sink pattern). Red cross symbols indicate the number of cycles leading to the cracks detection in the ceramic observed for highly curved assemblies at the initial time (>160 μm).

The bare substrate does not show any variation of its camber during the thermal cycles. Substrates with arrays and splined channels show a drastic decrease of their warpage of more than 50% after 1000 cycles. At the end of aging, deformations were less than 50 μm, and no visible cracks are detected in the substrate ceramic. However, the initially most curved substrates (castle border-like and linear channel heat sinks) show a limited decrease of their warpage of about 25%, and both of them present cracks in the brittle AlN ceramic once checked after 400 cycles. Since the substrate

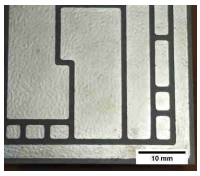

Fig. 11. Blisters macroscopic image on the top surface of the DBA substrate.

deformation is related to the residual stresses accumulated in the assembly, the stress relaxation during the creep of the aluminum-based alloy at high temperatures (above 25% of alloy melting temperature) is reflected by the reduction of the warpage value. However, the crack appearance after several hundred cycles in the highly curved assemblies can be related to the kinematic hardening of AlSiMg alloy under cyclic loads. The stresses induced by the CTE mismatch between the various materials increase progressively until locally reaching the ceramic fracture toughness [28].

Otherwise, after the first 100 cycles, blisters appear at the surface of the metal layer with an increase of the surface roughness, as shown in Fig. 11. This behavior has been already reported during the aging of DBA substrate, and it has been related to the shift of the grain joint in polycrystalline metal under plastic creep effect induced by high temperature, high tensile, and compressive stresses [29]. The high stresses are due to the CTE mismatch between the Al metallization (24 ppm/°C) and the AlN ceramic (4.5 ppm/°C). The roughness increase is due to the projection of Al grain from the surface during the thermal cycles. Choe *et al.* [30] have already shown that the roughness of the Al corresponds exactly to the grain joint profile and, more specifically, to the interfaces between the nondeformed grain and the projected grain. This issue should be considered in the future since it can impact the die attach reliability of the fully packaged power components.

C. Discussion and Recommendations for Harsh Environment Applications

Since the goal is to develop power modules that will be inserted in converters used as a power supply, to drive smart electrical machines and actuator in a nonpressurized environment, the assembly should withstand specific mechanical and thermal stresses related to the aeronautics requirements (depressurization, vibrations, mechanical shocks, large temperature swings, and high ambient temperature). The mechanical intrinsic properties, such as UTS and YS of the additive manufactured material, are higher than for the conventional casting material. In addition, the mechanical adhesion between the printed alloy and the metal layer of the substrate is very high, and values are about two folds higher than the components attached by solder (connectors, devices, and so on) [5], [31], [32]. Accordingly, the mechanical stresses due to the vibration and the mechanical shocks will not be considered as a potential issue for the future development of this technology.

The thermal performance is an important factor when designing and testing heatsinks. 3-D printing is a very promising technique since it allows to print more complicated

structures and to remove the TIM in order to reduce the heat resistance and increase the reliability under a harsh environment. However, we have shown that the $AlSi_7Mg_{0.6}$ alloy used in this study has a thermal conductivity of about 112 $W \cdot m^{-1} \cdot K^{-1}$. This value is lower than the aluminum one, commonly used to manufacture lightweight heat sinks. Based on thermofluid simulations, the authors have shown that, compared to conventional package using Al heat sink with pin fins, the direct printing or AlSiMg alloy with nonconventional design (water drop shape or elliptical shape) can allow the junction to ambient thermal resistance reduction by more than 20% for air-cooled heat sink [21]. In the future, additive manufactured copper with high thermal conductivity can be used to further decrease the thermal resistance of the printed material [33].

Otherwise, it has been shown that, for some heat sink designs, high residual stresses can be induced in the assembly after the additive manufacturing process. The high residual stresses are reflected with a high warpage value measured on the substrate and can lead to the reduction the assembly reliability under large thermal cycles. The heat sinks patterns with pin fins arrays using short continuous linear length are recommended to avoid the substrate bowing and the ceramic cracking during thermal cycles. However, in some cases (e.g., to print a channel for liquid cooling), the use of a continuous pattern is necessary. Continuous crooked or splined lines pattern can be successfully used. By using a suitable heat sink design, the packages show very promising results during thermal storage and thermal cycling tests. To the best of our knowledge, such robustness characteristics for a package, including the substrate and the heat sink, were not reported in the literature. Hence, this technology can pave the road to the development of electronic packaging with high thermal performance for harsh environment applications.

IV. Conclusion

Various heat sink patterns have been printed on a DBA metallized substrate using the SLM technique. The assemblies have been evaluated at the initial time and during harsh aging conditions. The bulk materials have shown good mechanical properties at the initial time and after 1000 h of aging at 200 °C. The interfaces between the laser melted $AlSi_7Mg_{0.6}$ alloy and Al metallization of the substrate have not shown any voids or fracture and have presented high mechanical adhesion with shear strength values exceeding 100 MPa. The aging under high-temperature storage and passive thermal cycling has not impacted the interface properties, and ductile fractures take place in the bulk of the Al substrate metal layer in almost all the cases before and after the aging conditions.

The influence of the heat sink patterns on the residual stresses in the assembly has been highlighted. Designs with long straight lines on the substrate have led to high residual stresses in the structure that causes the substrate warpage. Hence, it has been recommended to use fin array heat sink designs with noncontinuous patterns or continuous patterns with splined lines if necessary. The thermal cycles have allowed decreasing the cambers of the substrate due to the creep of the Al-based alloy at high temperatures. However, due to the hardening of the alloy, initially highly curved substrates (>150 μm) show cracks in ceramic after 400 cycles.

Finally, taking into consideration some heat sink designs, the direct printing of heat sinks on the DBA substrates has proved to be a very promising technology to develop high-performance and high-reliability power module packaging.

References

[1] K.-A. Son *et al.*, "GaN-based high temperature and radiation-hard electronics for harsh environments," *Nanosci. Nanotechnol. Lett.*, vol. 2, no. 2, pp. 89–95, Jun. 2010.

[2] T. Funaki *et al.*, "SiC JFET DC characteristics under extremely high ambient temperatures," *IEICE Electron. Exp.*, vol. 1, no. 17, pp. 523–527, 2004.

[3] A. Sakanova, C. F. Tong, A. Nawawi, R. Simanjorang, K. J. Tseng, and A. K. Gupta, "Investigation on weight consideration of liquid coolant system for power electronics converter in future aircraft," *Appl. Thermal Eng.*, vol. 104, pp. 603–615, Jul. 2016.

[4] R. Khazaka, L. Mendizabal, D. Henry, and R. Hanna, "Survey of high-temperature reliability of power electronics packaging components," *IEEE Trans. Power Electron.*, vol. 30, no. 5, pp. 2456–2464, May 2015.

[5] M. Knoerr, S. Kraft, and A. Schletz, "Reliability assessment of sintered nano-silver die attachment for power semiconductors," in *Proc. 12th Electron. Packag. Technol. Conf.*, Dec. 2010, pp. 56–61.

[6] S. W. Yoon, M. D. Glover, and K. Shiozaki, "Nickel–Tin transient liquid phase bonding toward high-temperature operational power electronics in electrified vehicles," *IEEE Trans. Power Electron.*, vol. 28, no. 5, pp. 2448–2456, May 2013.

[7] A. Fukumoto, D. Berry, and D. T. G.-Q. Ngo et Lu, "Effects of extreme temperature swings (−55 °C to 250 °C) on silicon nitride active metal brazing substrates," *IEEE Trans. Device Mater. Rel.*, vol. 14, no. 12, pp. 751–756, Jun. 2014.

[8] T. G. Lei, J. N. Calata, K. D. T. Ngo, and G.-Q. Lu, "Effects of large-temperature cycling range on direct bond aluminum substrate," *IEEE Trans. Device Mater. Rel.*, vol. 9, no. 4, pp. 563–568, Dec. 2009.

[9] A. Christmann and C. Mainka, "Facing high thermal loads on power modules in hybrid electrical vehicles," in *Proc. Int. Exhib. Conf. Power Electron., Intell. Motion, Renew. Energy Energy Manage. (PCIM)*, Nurenberg, Germany, 2010, pp. 432–438.

[10] R. Skuriat, J. F. Li, P. A. Agyakwa, N. Mattey, P. Evans, and C. M. Johnson, "Degradation of thermal interface materials for high-temperature power electronics applications," *Microelectron. Rel.*, vol. 53, no. 12, pp. 1933–1942, Dec. 2013.

[11] V.-N. Le, L. Benabou, Q.-B. Tao, and V. Etgens, "Modeling of inter-granular thermal fatigue cracking of a lead-free solder joint in a power electronic module," *Int. J. Solids Struct.*, vols. 106–107, pp. 1–12, Feb. 2017.

[12] J. Due and A. J. Robinson, "Reliability of thermal interface materials: A review," *Appl. Thermal Eng.*, vol. 50, no. 1, pp. 455–463, Jan. 2013.

[13] K. Forsback, "Reliability of thermal interface materials for power semiconductor devices," M.S. thesis, Dept. Elect. Eng. Automat., Aalto Univ., Espoo, Finland, 2017.

[14] C. Buttay *et al.*, "Compact inverter designed for high-temperature operation," in *Proc. IEEE Power Electron. Specialists Conf.*, Orlando, FL, USA, Jun. 2007, pp. 2241–2247.

[15] K. Gould, S. Q. Cai, C. Neft, and A. Bhunia, "Liquid jet impingement cooling of a silicon carbide power conversion module for vehicle applications," *IEEE Trans. Power Electron.*, vol. 30, no. 6, pp. 2975–2984, Jun. 2015.

[16] J. Kim, "Spray cooling heat transfer: The state of the art," *Int. J. Heat Fluid Flow*, vol. 28, no. 4, pp. 753–767, Aug. 2007.

[17] Y. Ding, Y. Li, Y. Li, W. Chen, H. Zhang, and D. Li, "Intensive cooling method for power electronic component with high heat flux," in *Proc. 13th Int. Conf. Control Autom. Robot. Vis. (ICARCV)*, Singapore, Dec. 2014, pp. 163–168.

[18] E. M. Dede, S. N. Joshi, and F. Zhou, "Topology optimization, additive layer manufacturing, and experimental testing of an air-cooled heat sink," *J. Mech. Des.*, vol. 137, no. 11, Nov. 2015, Art. no. 111403.

[19] M. Wong, I. Owen, C. J. Sutcliffe, and A. Puri, "Convective heat transfer and pressure losses across novel heat sinks fabricated by selective laser melting," *Int. J. Heat Mass Transf.*, vol. 52, nos. 1–2, pp. 281–288, Jan. 2009.

[20] A. Syed-Khaja, A. P. Freire, C. Kaestle, and J. Franke, "Feasibility investigations on selective laser melting for the development of microchannel cooling in power electronics," in *Proc. IEEE 67th Electron. Compon. Technol. Conf. (ECTC)*, Orlando, FL, USA, May 2017, pp. 1491–1496.
[21] R. Khazaka, D. Martineau, T. Youssef, T. L. Le, and S. Azzopardi, "Direct printing of heat sinks, cases and power connectors on insulated substrate using selective laser melting techniques," in *Proc. IEEE 69th Electron. Compon. Technol. Conf. (ECTC)*, Las Vegas, NV, USA, May 2019, pp. 2173–2179.
[22] A. Lindemann and G. Strauch, "Properties of direct aluminum bonded substrates for power semiconductor components," *IEEE Trans. Power Electron.*, vol. 22, no. 2, pp. 384–391, Mar. 2007.
[23] D. Manfredi *et al.*, *Additive Manufacturing of Al Alloys and Aluminium Matrix Composites (AMCs)*, Rijeka, Croatia: InTech, 2014.
[24] F. Trevisan *et al.*, "On the selective laser melting (SLM) of the AlSi10Mg alloy: Process, microstructure, and mechanical properties," *Materials*, vol. 10, no. 1, p. 76, Jan. 2017.
[25] L. P. Lam, D. Q. Zhang, Z. H. Liu, and C. K. Chua, "Phase analysis and microstructure characterisation of AlSi10Mg parts produced by selective laser melting," *Virtual Phys. Prototyping*, vol. 10, no. 4, pp. 207–215, Oct. 2015.
[26] D. Herzog, V. Seyda, E. C. Wycisk, and C. Emmelmann, "Additive manufacturing of metals," vol. 117, no. 1371, pp. 371–392, Sep. 2016.
[27] A. Mertens, O. Dedry, D. Reuter, O. Rigo, and J. Lecomte-Beckers, "Thermal treatments of AlSi10Mg processed by laser beam melting," in *Proc. 26th Int. Solid Freeform Fabr. Symp.*, Dayton, OH, USA, 2015, pp. 1007–1016.
[28] M. Khadyko, S. Dumoulin, T. Børvik, and O. S. Hopperstad, "An experimental–numerical method to determine the work-hardening of anisotropic ductile materials at large strains," *Int. J. Mech. Sci.*, vol. 88, pp. 25–36, Nov. 2014.
[29] C. Molteni, N. Marzari, M. C. Payne, and V. Heine, "Sliding mechanisms in aluminum grain boundaries," *Phys. Rev. Lett.*, vol. 79, no. 5, pp. 869–872, 1997.
[30] C. Choe, C. Chen, S. Noh, and K. Suganuma, "Thermal shock performance of DBA/AMB substrates plated by Ni and Ni–P layers for high-temperature applications of power device modules," *Materials*, vol. 11, no. 12, p. 2394, Nov. 2018.
[31] L. A. Navarro *et al.*, "Thermomechanical assessment of die-attach materials for wide bandgap semiconductor devices and harsh environment applications," *IEEE Trans. Power Electron.*, vol. 29, no. 5, pp. 2261–2271, May 2014.
[32] K. Kido, F. Momose, Y. Nishimura, and T. Goto, "Development of copper-copper bonding by ultrasonic welding for IGBT modules," in *Proc. 34th IEEE/CPMT Int. Electron. Manuf. Technol. Symp. (IEMT)*, Nov. 2010, pp. 1–5.
[33] T.-T. Ikeshoji, K. Nakamura, M. Yonehara, K. Imai, and H. Kyogoku, "Selective laser melting of pure copper," *J. Minerals, Metals Mater. Soc.*, vol. 70, no. 3, pp. 396–400, Mar. 2018.

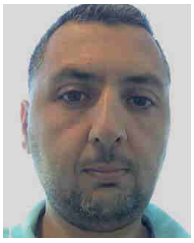

Rabih Khazaka received the B.S. degree in applied physics and the M.S. degree in nanophysics sciences from Lebanese University, Beirut, Lebanon, in 2005 and 2007, respectively, and the Ph.D. degree in materials science and electrical engineering from Paul Sabatier University, Toulouse, France, in 2011.

He is currently a Researcher with the Electronic and Electrical Systems Research Group, Safran Tech, Magny-Les-Hameaux, France. He is the author and a coauthor of 16 articles in international peer-reviewed scientific journals and one book chapter. He holds more than 15 patents in the field of materials and power electronic packaging. His current research fields focus on the study of materials, packaging technologies, and reliability modeling of power electronic modules for harsh environments.

Elodie Martin received the Engineering degree in materials from the École Nationale Supérieure des Ingénieurs en Arts Chimiques et Technologiques (ENSIACET), Toulouse, France, and Toulouse INP, Toulouse, in 2014, and the Ph.D. degree in science and materials engineering from the University of Toulouse, Toulouse, in 2018.

During her studies, she followed a specialization in materials and structures durability. She is currently with the Aeronautics, Space & Defense Division, Altran, Paris, France, and is working for the Materials Laboratory, Liebherr-Aerospace Toulouse SAS, Toulouse. She is the author or a coauthor of a publication and two international oral communications with acts.

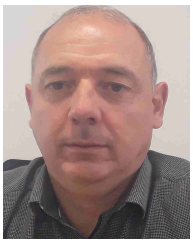

Joel Alexis received the master's degree in mechanical engineering from the National Engineering School of Tarbes, INP-ENIT, Tarbes, France, in 1995, the master's degree in materials science from Paul Sabatier University, Toulouse, France, in 1996, and the Ph.D. degree in materials science from the Institut National Polytechnique de Toulouse, Toulouse, in 2000.

In 2015, he obtained the position of Full Professor at the Production Engineering Laboratory, INP-ENIT. His research focused on the adhesion and mechanical properties of ZnNi deposits. He is the author or a coauthor of 44 articles in international peer-reviewed scientific journals and 63 presentations at national and international conferences. Since 2001, his main research interests include materials processing, advanced materials joining, and additive manufacturing.

Donatien Martineau received the M.Sc. degree in nanophysics sciences from Paul Sabatier University, Toulouse, France, in 2007, and the Ph.D. degree in materials science for electronic from the Graduate School of Engineering, INSA Toulouse, Toulouse, in 2011.

In 2016, he joined the Electronic and Electrical Systems Research Group, Safran Tech, Magny-Les-Hameaux, France, as a Researcher. He is the author or a coauthor of 13 articles in international peer-reviewed scientific journals. He holds more than eight patents in the field of materials and power electronic packaging. His current research fields focus on the study of power electronics reliability and packaging technologies.

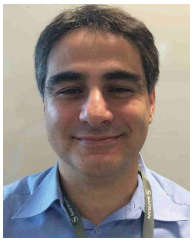

Stephane Azzopardi received the M.E. degree from the Graduate School of Engineering, INSA Toulouse, Toulouse, France, in 1993, the M.Sc. degree from Paul Sabatier University, Toulouse, in 1993, and the Ph.D. degree in electronics from the College of Science and Technology, University of Bordeaux, Bordeaux, France, in 1998.

In 2003, he became an Associate Professor at the Electrical Engineering Department, Bordeaux Institute of Technology, Bordeaux. He joined Safran Tech, Magny-Les-Hameaux, France, in September 2015. He manages the expert team on "power electronics" with a specific focus on more electrical aircraft and more electrical propulsion activities. As a senior expert on power modules, his research is focusing on the robustness of power semiconductor devices and the reliability of power modules for aeronautics applications.